PCCP

Cite this: *Phys. Chem. Chem. Phys.*, 2012, **14**, 9016–9025

www.rsc.org/pccp

PAPER

The effect of hydrogen bonding on the excited-state proton transfer in 2-(2′-hydroxyphenyl)benzothiazole: a TDDFT molecular dynamics study†

Nawee Kungwan,*[ab] Felix Plasser,[b] Adélia J. A. Aquino,[bcd] Mario Barbatti,[e] Peter Wolschann[b] and Hans Lischka*[bd]

Received 6th December 2011, Accepted 16th March 2012
DOI: 10.1039/c2cp23905a

The dynamics of the excited-state proton transfer (ESPT) in a cluster of 2-(2′-hydroxyphenyl)-benzothiazole (HBT) and hydrogen-bonded water molecules was investigated by means of quantum chemical simulations. Two different enol ground-state structures of HBT interacting with the water cluster were chosen as initial structures for the excited-state dynamics: (i) an intramolecular hydrogen-bonded structure of HBT and (ii) a cluster where the intramolecular hydrogen bond in HBT is broken by intermolecular interactions with water molecules. On-the-fly dynamics simulations using time-dependent density functional theory show that after photoexcitation to the S_1 state the ESPT pathway leading to the keto form strongly depends on the initial ground state structure of the HBT–water cluster. In the intramolecular hydrogen-bonded structures direct excited-state proton transfer is observed within 18 fs, which is a factor two faster than proton transfer in HBT computed for the gas phase. Intermolecular bonded HBT complexes show a complex pattern of excited-state proton transfer involving several distinct mechanisms. In the main process the tautomerization proceeds *via* a triple proton transfer through the water network with an average proton transfer time of approximately 120 fs. Due to the lack of the stabilizing hydrogen bond, intermolecular hydrogen-bonded structures have a significant degree of interring twisting already in the ground state. During the excited state dynamics, the twist tends to quickly increase indicating that internal conversion to the electronic ground state should take place at the sub-picosecond scale.

1 Introduction

Proton transfer (PT) and hydrogen transfer (HT) processes play an important role in chemistry and biochemistry.[1,2] In particular, excited-state intramolecular proton transfer (ESIPT)[3] has been intensively studied due to its practical use in laser dyes, photo-stabilizers,[4] fluorescent probes in bioimaging[5–7] and light-emitting devices.[8,9] Most of the ESIPT processes occur in molecules possessing a strong intramolecular hydrogen bond between O–H (or N–H) and C=O or pyridinic nitrogen groups, in which the intrinsic PT from the enol to keto form in the ππ* state is barrierless in gas-phase and non-polar solvents.[10] Details of ESIPT are both theoretically and experimentally well-documented and understood for several cases such as 2-(2′-hydroxyphenyl)benzothiazole (HBT),[10–19] 2-(2′-hydroxyphenyl)benzoxazole (HBO),[20,21] 10-hydroxybenzo[h]quinoline (HBQ),[22–24] 2-(2′-hydroxyphenyl)benzotriazole (TIN-H),[25,26] and [2,2′-bipyridyl]-3,3′-diol ($BP(OH)_2$).[27–29] For a general review on hydrogen bonding in the excited state see *e.g.* ref. 30.

HBT has served as a prototype of ESIPT and has been extensively studied by many groups.[11–14,17,31,32] Comprehensive analysis of the ESIPT mechanism and subsequent internal conversion pathway in gas phase was recently reported based on femtosecond experiments and theoretical dynamics simulation.[18] In gas phase and non-polar solvents, the absorption spectrum of HBT has a maximum around 340 nm due to the enol tautomer, while the fluorescence spectrum has a maximum around 550 nm due to the keto tautomer. The large Stokes shift between the enol and keto forms documents the structural changes occurring during the ESIPT. Moreover, the location of the keto fluorescence band is practically solvent independent in the case of non-polar media.[10] As long as the intramolecular hydrogen bond in HBT exists, ESIPT should occur at a similar

[a] *Department of Chemistry, Faculty of Science, Chiang Mai University, Chiang Mai 50200, Thailand. E-mail: naweekung@hotmail.com*
[b] *Institute for Theoretical Chemistry, University of Vienna, Währinger Straße 17, A-1090 Vienna, Austria*
[c] *Institute of Soil Research, University of Natural Resources and Life Sciences, Peter-Jordan-Straße 82, A-1190 Vienna, Austria*
[d] *Department of Chemistry and Biochemistry, Texas Tech University, Lubbock, Texas 79409-1061, USA. E-mail: hans.lischka@ttu.edu*
[e] *Max-Planck-Institut für Kohlenforschung, Kaiser-Wilhelm-Platz 1, D-45470, Mülheim an der Ruhr, Germany*

† Electronic supplementary information (ESI) available: Ground state optimized structures of the intramolecular hydrogen-bonded HBT–(H_2O) complex computed at the DFT/B3LYP/SVP-SV level, Cartesian geometries of structure on HBT–$(H_2O)_{1-3}$ complexes at B3LYP, RI-MP2 and RI-CC2 levels computed with the TZVP-sp basis set. See DOI: 10.1039/c2cp23905a

time scale either in gas phase or in non-polar solvents, for which values about 50 fs have been determined.[33] In polar solvents forming hydrogen bonds, two fluorescence bands are observed, one around 380 nm corresponding to the enol form and a weak band due to the keto form around 550 nm.[10,17,34] The lack of keto emission in a polar solvent is considered to be caused by intermolecular hydrogen bonding of the OH group of HBT to solvent molecules which is competing with intramolecular hydrogen bonding. Additionally, in protic solvents, especially in ethanol or water, fluorescence bands of deprotonated anionic, neutral enol or protonated cationic forms have been also observed.[17] This observation could be explained as a proton transfer catalyzed by a solvent bridge or by charge transfer processes. Concerning the occurrence of *cis*- and *trans*-keto HBT species, experimental evidence suggests that a *trans*-keto structure is observed only in non-hydrogen bonding solvents whereas in the case of water (and other protic solvents) either intramolecular proton transfer in the *cis* form or the above-mentioned proton transfer to the solvent occurs.[32]

Understanding the mechanism of excited-state proton transfer (ESPT) through a solvent bridge requires knowledge on the structure of hydrogen-bonded complexes. Experiments have been performed for small solvent clusters in a supersonic jet together with analysis by laser spectroscopy.[35–37] These experiments have provided information on stoichiometry and stability of different hydrogen-bonded species. The solvent-assisted excited-state proton transfer mechanism involves possibly several pathways through complicated hydrogen-bonded networks, intermediates and transition states along the reaction path. Recently, proton/hydrogen transfer reactions in the excited state were studied for phenol with water and ammonia,[38] for 7-azaindole with water (7AI/H_2O),[39–42] alcohol,[37,43–46] and ammonia (7AI/NH_3),[47] for 7-hydroxylquinoline with alcohol,[48–50] water (7HQ/H_2O),[51] and ammonia (7HQ/NH_3),[52,53] for 7-hydroxy-4-methylcoumarin with water,[54] for 6-hydroxyquinoline with acetic acid[55] and for 1*H*-pyrrolo[3,2*h*]quinoline with water (PQ/H_2O)[36] and with methanol (PQ/MeOH).[35] Furthermore, *ab initio* molecular dynamic studies on ESPT of 7AI in aqueous solution[56] and methanol[46] and of 7HQ in ammonia cluster[57] have been performed. Such dynamics studies can provide detailed mechanistic information on pathways and proton-transfer time scales.

It is the aim of the present work to examine the excited-state proton transfer reaction in HBT within a water cluster environment by static and dynamics simulations. The effect of intermolecular hydrogen bonding can occur in two ways. In the electronic ground state, the intramolecular hydrogen bond in HBT can be broken by surrounding water molecules (see *e.g.* ref. 15) and the proton transfer dynamics in the excited state will be influenced by the surrounding water network. Therefore, detailed information on different ground-state complexes of HBT hydrogen-bonded with water is required in the first place, prior to the dynamics simulation of the ESPT. Two different types of cluster structures in the electronic ground state can be envisaged: in the first, the intramolecular hydrogen bond in HBT is surrounded by water molecules (intramolecular hydrogen-bonded HBT); in the second, the intramolecular hydrogen bond in HBT is broken, and the –OH group and the –N atom of HBT are connected through a network of water molecules (intermolecular hydrogen-bonded HBT). Sampling the entire structural manifold with interconversion of intra- and intermolecular hydrogen-bonded HBT is far too costly at the quantum mechanical level. Therefore, several possible ground state structures were compared to choose appropriate candidates for those two types of structures. Subsequently, the proton/hydrogen transfer pathways through this water network are followed through excited-state dynamics calculations. Similar simulations have already been carried out previously for isolated HBT[18,22] using time-dependent density functional theory (TDDFT). The goal of the present simulations is to understand the different reaction pathways in the water-cluster environment and to determine the corresponding time constants. The question of hydrogen transfer *vs.* proton transfer will also be addressed in this paper.

2 Computational details

Ground state optimizations were carried out for HBT–$(H_2O)_n$ (n = 1–3) clusters using density functional theory (DFT) with the B3LYP functional[58,59] with two different basis sets, SVP-SV and TZVP + sp. The SVP-SV basis set is defined as the split valence polarized (SVP)[60] basis assigned to heavy atoms and hydrogen atoms involved in the hydrogen-bonded network of a complex and a split valence (SV) basis used for the remaining hydrogen atoms and the four carbon atoms in the thiazole ring. For the TZVP + sp basis,[61] diffuse functions (s,p) are added to the triple-ζ valence polarized (TZVP)[60] basis set for atoms that are involved in the hydrogen-bonded network, in analogy to the procedures presented in ref. 61. The character of optimized structures as energy minima was confirmed by the absence of imaginary vibrational frequencies computed in the harmonic approximation. Resolution-of-the-identity Møller–Plesset perturbation theory[62] to second-order (RI-MP2)[63,64] calculations were performed to obtain reference structures for hydrogen-bonded complexes. Moreover, the approximate coupled cluster singles-and-doubles method using the RI method (RI-CC2)[65–67] with the SVP-SV basis set was also employed for geometry optimizations. All B3LYP, RI-MP2 and RI-CC2 calculations were carried out using the Turbomole program package.[68] Furthermore, thermodynamic data for the electronic ground state were computed at 273 K using the harmonic oscillator/rigid rotator/ideal gas model.

Excited-state calculations were performed primarily by means of the TDDFT method.[69–72] Selected geometries have been re-computed at the RI-CC2 level. In previous investigations,[22,26,73] it has been shown that the RI-CC2 method is very well suited to provide benchmark results to assess possible artifacts of the TD-DFT method. Comparisons for a series of ESIPT cases including HBT[22,73] demonstrated that TD-DFT gives quite reliable results for the proton transfer process in the ππ* state.

Classical dynamics simulations were carried out for HBT–$(H_2O)_3$ on the energy surface of the first excited singlet state S_1. Fifty trajectories were computed with a time step of 0.5 fs and the maximum time up to 100 fs for intramolecular hydrogen-bonded HBT and 300 fs for intermolecular hydrogen-bonded HBT. The initial conditions for each trajectory were generated using a Wigner distribution of the ground state vibrational quantum harmonic-oscillator in the electronic ground state. The excited-state dynamics calculations were performed at the TDDFT/B3LYP/SVP-SV level using the NEWTON-X program[74,75] interfaced with TURBOMOLE.

3 Results and discussion

3.1 Ground state structure

To understand the influence of the surrounding water molecules on the hydrogen bond in HBT, HBT–$(H_2O)_n$ (n = 1–3) complexes were optimized at the RI-MP2, RI-CC2 and B3LYP levels using different basis sets. Geometric and energetic characterization of each cluster is presented in the following sections.

3.1.1 HBT–(H_2O) complex. The HBT–(H_2O) cluster is optimized by letting a water molecule approach HBT to give the intramolecular hydrogen-bond form. The optimized structure computed at the B3LYP/SVP-SV level with atom numbering of the intramolecular hydrogen-bonded HBT–(H_2O) complex is depicted in Fig. 1a. The intramolecular hydrogen bond is characterized by a N···H1 bond length of 1.644 Å as given in Table 1. It is shorter in HBT–(H_2O) by 0.071 Å than that in isolated HBT (the N···H1 bond length in isolated HBT is 1.715 Å). The N···H3 distance shows a relatively strong dependence on the method and basis set. This sensitivity seems to be connected to coupling with the NCCC torsional angle, which is larger for the larger basis set (see Table 1, RI-MP2 results, intramolecular complex) and the intramolecular N···H1 bond length. The latter distance increases with increasing torsional angle, allowing a closer approach of the water hydrogen to the nitrogen atom of HBT. Subtle differences in the environment induced by the use of different methods and basis sets seem to have nonnegligible influence particularly on the relatively weak N···H3 bond in comparison to the stronger N···H1 bond. The structure computed with the DFT/B3LYP/SVP-SV method is different (see Fig. S1 of the ESI†) with the water molecule bisecting the molecular plane of HBT. A reduced dependence of hydrogen bonding distances on the computational method is observed for the intramolecular two-water complex (Table 2). For the three-water complex (Table 3) different locations for the interaction of water molecules with HBT and among themselves seem to be relatively saturated and basis set effects are not so pronounced anymore.

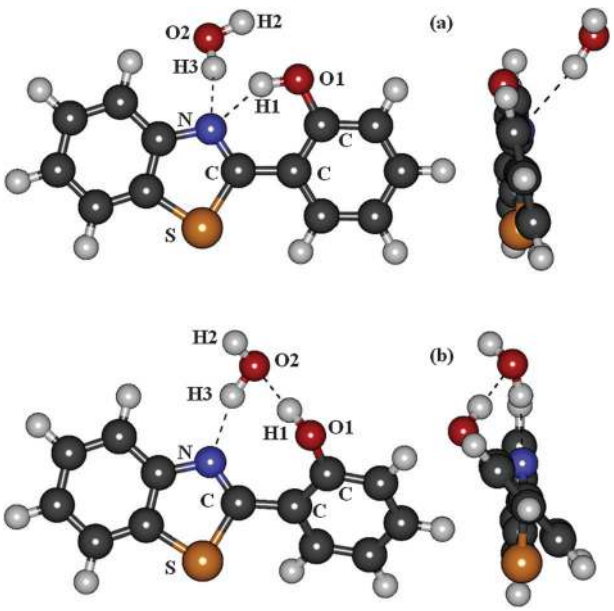

Fig. 1 A frontal and side view of the ground state optimized structures of the HBT–(H_2O) complex computed at the DFT/B3LYP/TZVP + sp level and atom numbering scheme. (a) Intramolecular hydrogen-bonded complex, (b) intermolecular complex.

Table 1 Selected bond lengths (Å), bond angles (°) and relative energies (kcal mol^{-1}) of HBT intramolecular and intermolecular hydrogen-bonded complexes with one water molecule computed at different levels of theory

	B3LYP		RI-MP2		RI-CC2
	SVP-SV	TZVP + sp	SVP-SV	TZVP + sp	SVP-SV
Intramolecular hydrogen-bonded complex					
r(N···H1)	1.644	1.791	1.720	1.798	1.779
r(N···H3)	2.551[a]	2.222	2.414	1.993	2.145
øNCCC	0	11	12	25	0
øSCCC	0	13	14	26	0
Intermolecular hydrogen-bonded complex					
r(N···H3)	1.664	1.744	1.696	1.740	1.625
r(O1···H2)	3.050	3.247	3.112	3.325	3.067
r(O2···H1)	1.782	1.829	1.831	1.813	1.762
r(N···H1)	2.639	2.692	2.720	2.795	2.614
øNCCC	38	43	51	59	38
øSCCC	39	44	51	59	38
ΔE^b	3.66	3.95	2.96	2.21	2.99

[a] Distance H3···O1 (see Fig. S1 in the ESI). [b] Energy differences (including ZPE correction) of the intermolecular hydrogen-bonded complex relative to the intramolecular complex.

The intermolecular hydrogen-bonded HBT–(H_2O) cluster is obtained by forming a hydrogen bond between the water molecule and the hydroxyl group of HBT. The optimized structure at B3LYP/SVP-SV with atom numbering of the intermolecular hydrogen-bonded HBT–(H_2O) cluster is depicted in Fig. 1b. From this figure, the intramolecular hydrogen bond N···H1 (bond length 1.644 Å) of the intramolecular hydrogen-bonded HBT–(H_2O) (Fig. 1a) is replaced by a new hydrogen bond O2···H1 (bond length 1.782 Å). A second intramolecular hydrogen bond N···H3 is also formed by rotating the H3 atom of the water molecule into the vicinity of the N atom of HBT. All approaches give the same type of interaction as shown in Fig. 1a and b. However, due to the

Table 2 Selected bond lengths (Å), bond angles (°) and relative energies (kcal mol^{-1}) of HBT intramolecular and intermolecular hydrogen-bonded complexes with two water molecules computed at different levels of theory

	B3LYP		RI-MP2		RI-CC2
	SVP-SV	TZVP + sp	SVP-SV	TZVP + sp	SVP-SV
Intramolecular hydrogen-bonded complex					
r(N···H1)	1.738	1.810	1.794	1.823	1.787
r(N···H2)	2.324	2.159	2.130	1.947	2.155
r(O2···H4)	1.837	1.882	1.854	1.854	1.856
øNCCC	10	14	19	29	18
øSCCC	12	17	21	29	21
Intermolecular hydrogen-bonded complex					
r(N···H1)	2.573	2.486	2.602	2.718	2.580
r(O2···H1)	1.712	1.921	1.744	1.797	1.717
r(O3···H2)	1.781	1.897	1.833	1.884	1.819
r(N···H4)	1.862	1.930	1.897	1.871	1.878
øNCCC	35	41	48	61	46
øSCCC	33	40	47	60	45
ΔE^a	1.43	−0.02	−0.36	−0.23	0.99

[a] Energy differences (including ZPE correction) of the intermolecular hydrogen-bonded complex relative to the intramolecular complex.

Table 3 Selected bond lengths (Å), bond angles (°) and relative energies (kcal mol^{-1}) of HBT intramolecular and intermolecular hydrogen-bonded complexes with three water molecules computed at different levels of theory

	B3LYP		RI-MP2		RI-CC2
	SVP-SV	TZVP + sp	SVP-SV	TZVP + sp	SVP-SV
Intramolecular hydrogen-bonded complex					
r(N–H1)	1.676	1.682	1.730	1.758	1.730
r(O1–H6)	2.002	1.998	1.992	1.948	1.991
r(O2–H4)	1.757	1.867	1.783	1.842	1.785
r(O3–H7)	1.953	2.078	2.024	2.114	2.027
r(O4–H3)	1.799	1.854	1.862	1.975	1.865
øSCCC	7	1	19	20	20
øNCCC	5	1	16	24	19
Intermolecular hydrogen-bonded complex					
r(N–H1)	2.617	2.587	2.642	2.820	2.618
r(N–H4)	1.935	2.085	2.031	1.985	2.008
r(O1–H6)	1.807	1.914	1.863	1.826	1.862
r(O2–H1)	1.517	1.817	1.670	1.740	1.648
r(O3–H3)	1.613	1.812	1.747	1.800	1.729
r(O4–H5)	1.742	1.927	1.838	1.893	1.829
øSCCC	30	40	53	73	50
øNCCC	32	41	53	73	50
ΔE^a	2.46	5.02	−0.68	0.64	0.57

[a] Energy differences (including ZPE correction) of the intermolecular hydrogen bonded complex relative to the intramolecular complex.

relatively weak interactions a significant scattering of the hydrogen bonded distances collected in Table 1 is observed. The interring torsional angles NCCC and SCCC in HBT show quasi-planarity for the intramolecular hydrogen-bonded structure but a stronger out-of-plane twist for the intermolecular hydrogen-bonded structure. The reason for this behavior is the larger flexibility of the intermolecular hydrogen bonds as compared to the intramolecular hydrogen bond.

The relative energies including ZPE correction of the investigated complexes given in Fig. 1a and b are shown in Table 1. The relative energy difference of 2.21 kcal mol^{-1} (RI-MP2/TZVP + sp) shows a favoring of the intramolecular hydrogen bonded structure.

3.1.2 HBT–$(H_2O)_2$ complex. When two water molecules are added to the HBT molecule a larger number of structural isomers can be expected. In Fig. 2a the lowest energy conformation found is displayed. The structure optimized at the B3LYP/SVP-SV level shows that the one water molecule forms a hydrogen bond to the nitrogen atom of HBT and the other water is hydrogen-bonded to the first one with a hydrogen bond O2···H4 of 1.837 Å (Table 2, B3LYP/SVP-SV). The second water acts as the hydrogen bond donor for the first one.

For the intermolecular hydrogen-bonded complex, the optimized structure at the B3LYP/TZVP + sp level shows that when the second water molecule is added, three hydrogen bonds O2···H1, O3···H2 and N···H4 are formed (Fig. 2b). The first water molecule still forms the hydrogen bond with the OH group of HBT (O2···H1) but not with the nitrogen atom since this bond is replaced by one belonging to the second water molecule. This second water molecule makes hydrogen bonds to the first water molecule and to the nitrogen atom establishing a hydrogen network of the HBT–$(H_2O)_2$ complex. All methods also show a stronger interring torsion in HBT for the intermolecular hydrogen-bonded complex as compared to the intramolecular one. The comparison

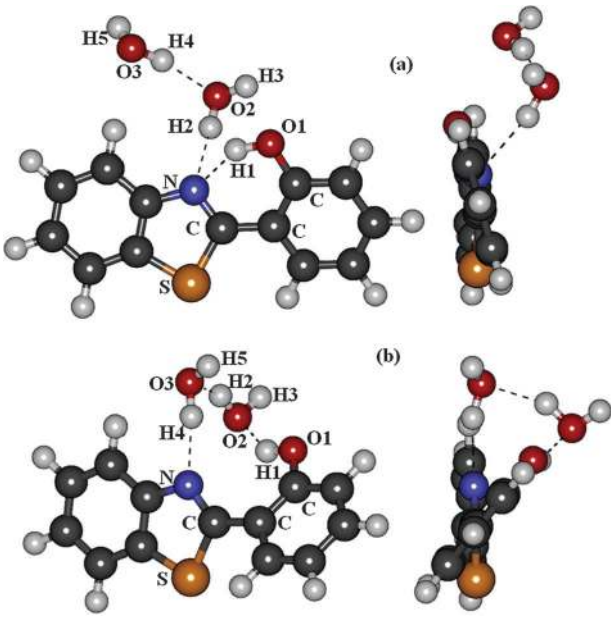

Fig. 2 A frontal and side view of the ground state optimized structures of the HBT–$(H_2O)_2$ complex computed at the DFT/B3LYP/TZVP + sp level and atom numbering scheme. (a) Intramolecular hydrogen-bonded complex. (b) Intermolecular complex.

of optimized structures computed with different methods shows relatively good global agreement, with some improvement over the situation of the one-water complexes.

The relative energies including ZPE correction of the investigated complexes given in Fig. 2a and b are collected in Table 2. The data show practical equal stability of the two types of complexes.

3.1.3 HBT–$(H_2O)_3$ complex. Starting from the intramolecular hydrogen-bonded HBT–$(H_2O)_2$ complex, the third water can be added into various positions and several minima on the shallow potential energy surface may be expected. Here we present only the structure of lowest energy based on B3LYP/SVP-SV calculations, which is displayed in Fig. 3a. The addition of a third water molecule to the HBT–$(H_2O)_2$ complex increases the number of hydrogen bonds between HBT and the water molecules. The third water forms three new hydrogen bonds to the original HBT–$(H_2O)_2$ complex, namely (O1···H6), (O3···H7) and (O4···H3) with bond lengths of 2.002, 1.953, and 1.799 Å, respectively (see Table 3). The other hydrogen bonds which still remain intact from the starting HBT–$(H_2O)_2$ complex are (N···H1) and (O2···H4) with bond lengths of 1.676 Å and 1.757 Å, respectively.

For the intermolecular hydrogen-bonded structure, by adding the third water molecule to the HBT–$(H_2O)_2$ complex, the arrangement of the HBT–$(H_2O)_3$ complex formed is depicted in Fig. 3b. Based on the results calculated at the B3LYP/SVP-SV level, there are five hydrogen bonds established between HBT and the three water molecules with bond lengths of 1.935 Å (N···H4), 1.807 Å (O1···H6), 1.517 Å (O2···H1), 1.613 Å (O3···H3), and 1.742 Å (O4···H5), respectively. As discussed for the previous complexes, the HBT interring torsion shows a strong twist for the intermolecular hydrogen-bonded complex. The relative energies including ZPE correction of investigated complexes given in Fig. 3a and b are shown in Table 3.

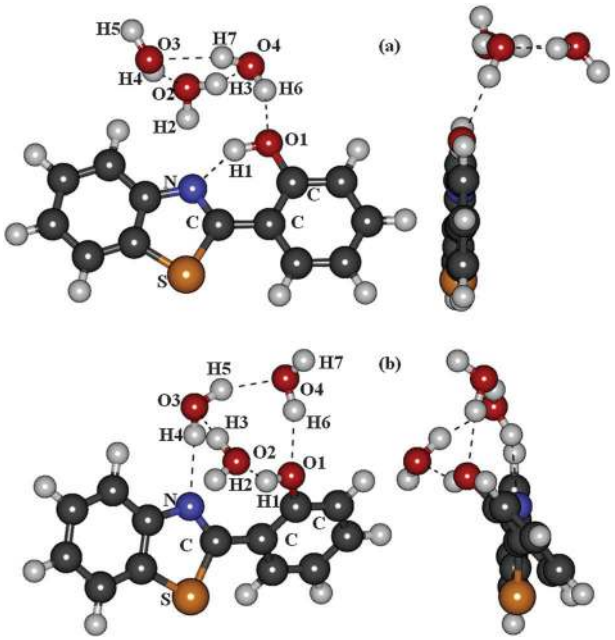

Fig. 3 A frontal and side view of the ground state optimized structures of the HBT–$(H_2O)_3$ complex computed at the DFT/B3LYP/TZVP + sp level and atom numbering scheme. (a) Intramolecular hydrogen-bonded complex. (b) Intermolecular complex.

For the proton transfer dynamics calculations, the HBT–$(H_2O)_3$ complexes were used since these clusters form already a sufficiently complex hydrogen-bonded network between the water molecules and HBT, which should be well representing the immediate hydration shell around HBT. The intramolecular and intermolecular structures discussed above have been selected as starting points for studying the different types of proton transfer processes occurring in the excited state. In addition, the ground state structures optimized at the B3LYP/SVP-SV level are for the most important structural parameters in quite good agreement with higher level theory and bigger basis sets. These results suggest that the cost effective B3LYP method with the SVP-SV basis set can be used in the following dynamic investigation.

3.2 TDDFT molecular dynamics results

On-the-fly dynamics simulations on the S_1 excited state were performed starting from both intermolecular and intramolecular hydrogen-bonded complexes of HBT–$(H_2O)_3$ at the TDDFT/B3LYP/SVP-SV level. A general analysis of the excited-state dynamics simulation analysis of both cases is summarized in Table 4. The results are discussed in the next sections.

3.2.1 Dynamics starting at the intramolecular hydrogen-bonded cluster. The atom numbering scheme for the intramolecular hydrogen-bonded complex of HBT–$(H_2O)_3$ is displayed in Fig. 3a. This scheme is used to describe the character of the proton transfer dynamics as shown in Fig. 4 and plotted in Fig. 5. The structural changes along the excited-state intramolecular proton transfer (ESIPT) pathway are given in Fig. 4 for a selected representative trajectory at 0 fs (initial enol structure), 20 fs (intermediary structure, IS) and 25 fs (keto structure). The ESIPT process starts with the proton from the O1 atom moving towards the N atom (as indicated by an arrow) through the intermediary structure IS in a barrierless reaction as in isolated HBT. The ESIPT process occurs for all 50 trajectories within the maximum time of dynamics simulation (100 fs, see Table 4).

Table 4 Summary of excited-state dynamics simulation analysis of both intramolecular and intermolecular hydrogen-bonded starting clusters[a]

			Proton transfer time/fs		
Initial tautomer	Process	Fraction (%)	PT1	PT2	ESPT
Intra	ESIPT	100	—	—	18
Inter	ESInterPT-2W	76	10	46	116
	IC	10	—	—	—
	BPT	8	—	—	—
	ESInterPT-1W	4	105	—	115
	ESIPT	2	—	—	205

[a] For definition of processes see the text.

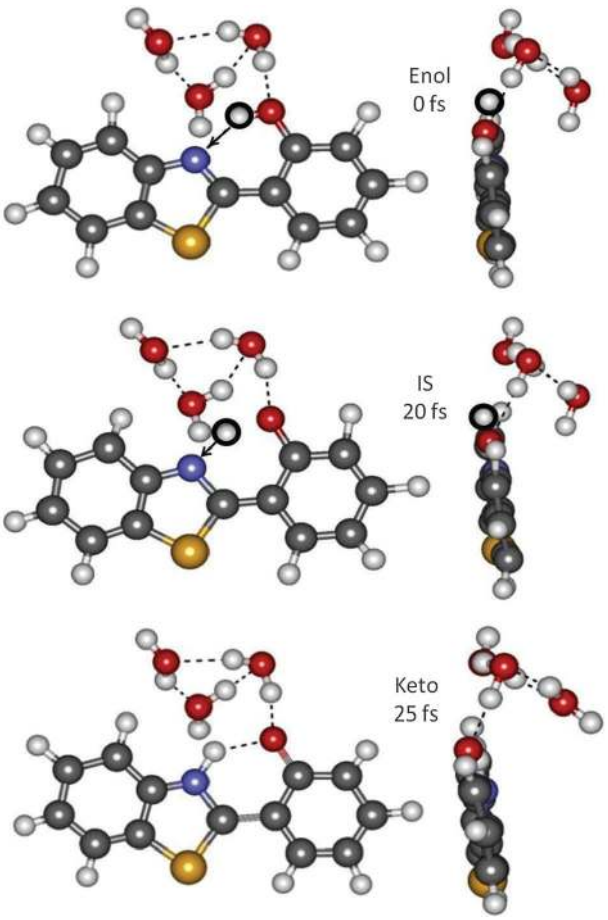

Fig. 4 A frontal and side view of the structures along the ESIPT pathway of a representative trajectory starting in the intramolecular hydrogen-bonded complex (left: front view, right: side view).

In Fig. 5a, the evolution of the average distances O1–H1 and N–H1, which characterize the proton transfer, is reported. The time for the proton transfer is defined as the average time for which the O1···H1 and N···H1 distances are equal. This is the same criterion adopted in the previous investigations of the proton transfer in HBT in gas phase[18] and in 7AI with methanol complexes.[46] During the initial 20 fs, the O1–H1 bond increases rapidly and at the same time the N–H1

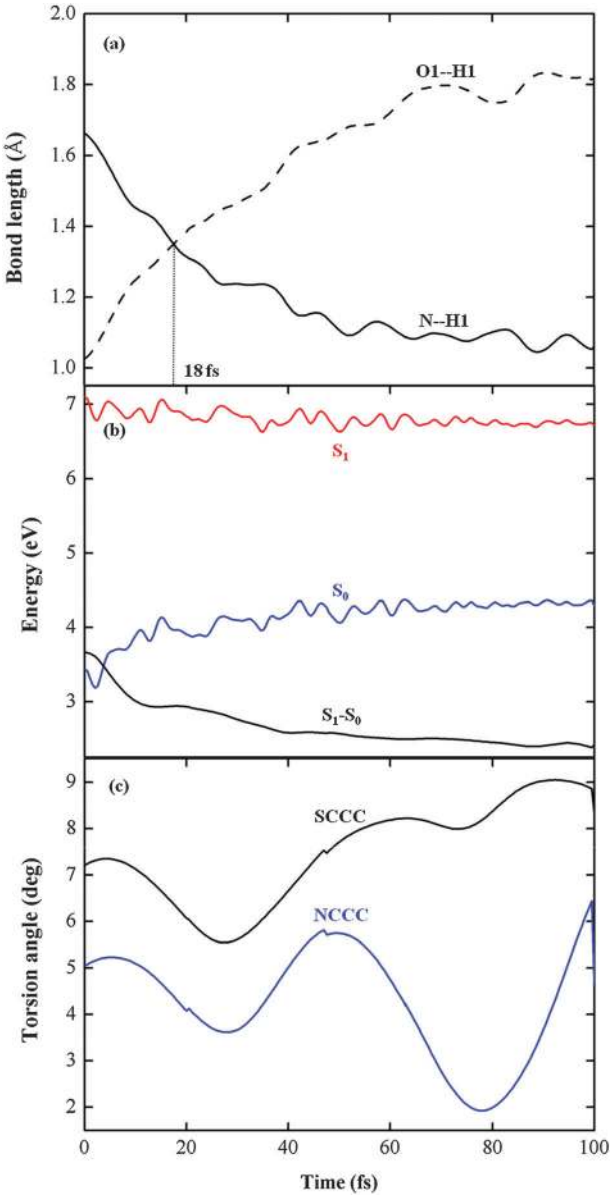

Fig. 5 (a) Time evolution of average bond breaking (O···H) and bond forming (N···H) distances. (b) Average S_1 and S_0 energies and average energy differences between S_1 and S_0 states. (c) Average torsional angles SCCC and NCCC.

decreases to form the new covalent NH bond, indicating that the ESIPT process has been accomplished. After 40 fs, the bond distances N–H1 and O1–H1 remain constant with an oscillation time period of 10 fs corresponding to the normal vibration of the N–H1 stretching mode. The averaged proton transfer time is about 18 fs, which is a factor two faster than that computed at the same level in the gas phase. This can be explained by the stronger hydrogen bond in the HBT–$(H_2O)_3$ complex (N···H1 = 1.676 Å) than that in isolated HBT (N···H1 = 1.715 Å), as shown in the ESI.†

In Fig. 5b, the time evolution of the average potential energy of S_1 and S_0 and the average difference energy of S_1 and S_0 are shown. The average energy difference is always larger than 2.5 eV revealing that no approach to a conical intersection between the two states occurs within the simulation time. This is in agreement with the time evolution of torsion angles SCCC and NCCC shown in Fig. 5c, whose values below 10° imply that the HBT structure is slightly twisted and still rather close to planarity. Moreover, we have extended the dynamics of one subset of 10 trajectories for 400 more femtoseconds. All of them twisted up to reaching the S_1/S_0 crossing. This leads to the expectation that for longer time scales an orthogonal structure will be accessed similar to what was found for the isolated HBT.[18]

3.2.2 Dynamics starting at the intermolecular hydrogen-bonded cluster. On-the-fly dynamics simulations were carried out for 50 trajectories starting at the intermolecular hydrogen-bonded cluster. A total of 38 trajectories (76%) showed excited-state intermolecular proton transfer through two water molecules (ESInterPT-2W). Five trajectories (10%) reached a crossing between the S_1 and S_0 states before any proton transfer (IC). Other four of them (8%) returned to the enol form through a back proton transfer (BPT). Two trajectories (4%) presented excited-state intermolecular transfer through one water molecule (ESInterPT-1W). In the last trajectory (2%), the structure changed from intermolecular hydrogen-bonded to intramolecular hydrogen-bonded and intramolecular proton transfer (ESIPT) occurred. The fractions for all these processes are summarized in Table 4. The following analysis will focus only at the dominant process, the excited-state intermolecular proton transfer through two water molecules (ESInterPT-2W).

The atom numbering scheme for the intermolecular hydrogen-bonded form of HBT–$(H_2O)_3$ is given in Fig. 3b. The structures along the reaction pathway are depicted in Fig. 6 for a representative trajectory as enol at 0 fs, IS1 at 15 fs, PT1 at 18 fs, IS2 at 47 fs, PT2 at 51 fs, IS3 at 112 fs, keto at 115 fs, and keto 90° twisted at 207 fs. The proton transfer process (indicated by an arrow) can be summarized by the following three steps: (1) H1 moves from O1 to O2, (2) H3 moves from O2 to O3 and (3) H4 moves from O3 to N. The tautomerization with water assistance is completed. The number of water molecules involved in the proton transfer mechanism is two, the third water molecule does not participate in the proton transfer process. The contribution of the third water molecule could be viewed as the hydrogen bonded network holder. Its role is to enhance the hydrogen-bonded network used for excited-state intermolecular proton transfer through two water molecules.

The time evolution of the three bond-forming distances O2···H1, O3···H3 and N···H4 and of the three bond-breaking distances O1···H1, O2···H3 and O3···H4 along the proton transfer pathway of the ESInterPT-2W process averaged over the 38 trajectories is shown in Fig. 7a. We adopt the same definition for X–H–Y proton transfer for all processes, where X is the proton donor (X–H breaking bond) and Y is the proton acceptor (Y–H forming bond). The time for the PT is determined as the time in which X–H and Y–H become equal. Along the dynamics, the three bond-forming distances decrease to covalent bond lengths and at the same time the three breaking interatomic distances increase as the respective covalent bond is being broken. At 10 fs, the average values of O1···H1 and O2···H1 bond distances are equal which gives the time for the first proton transfer (PT1) process. The second proton transfer (PT2) takes

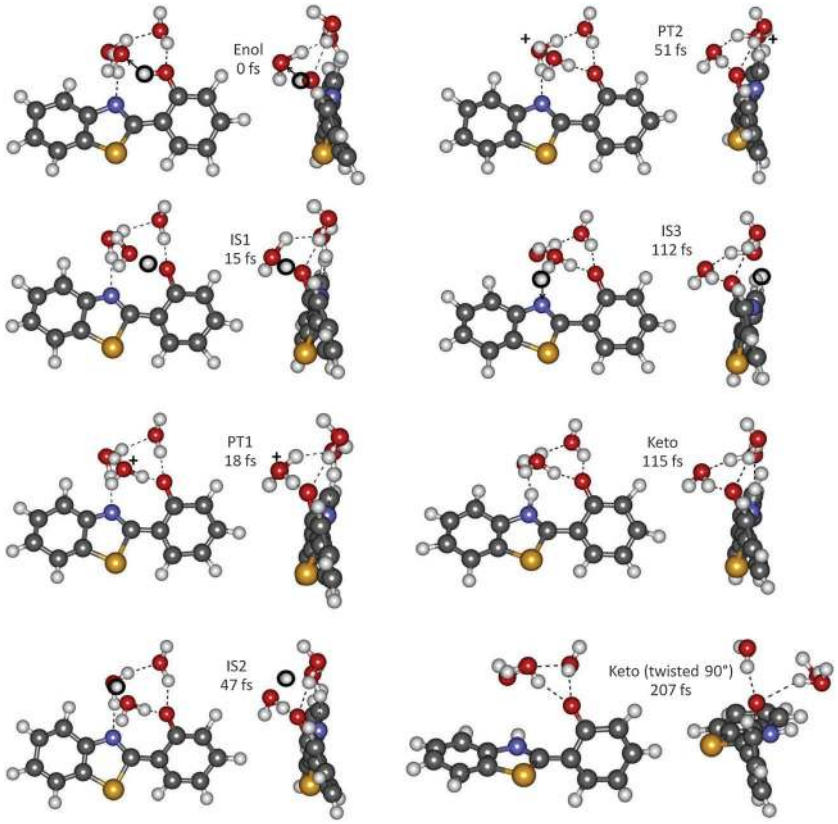

Fig. 6 Structures along the ESinterPT-2W pathway of a representative trajectory starting in the intermolecular hydrogen-bonded complex (left: front view, right: side view).

place at 46 fs as at this time the averaged bond distances of O2···H3 and O3···H3 are equal. Finally, the third proton transfer (PT3) occurs at about 116 fs when the averaged bond distances of O3···H4 and N···H4 are equal. After 100 fs the O2···H1 and the O3···H3 distances perform already oscillations around equilibrium values. N···H4, however, is still in the process of contraction at 150 fs.

After the completion of the cycle of the proton transfer process is reached, the relative energy difference of S_1–S_0 (Fig. 7b) gradually starts to decrease. This relative energy difference drops to below 2 eV due to the non-planar conformations of HBT (Fig. 7c). As in the gas phase case,[18] this is an indication that the internal conversion to the ground state is initiated.

The torsional angles SCCC and NCCC increase during the proton transfer process as shown in Fig. 7c, indicating that a twisting of the skeleton structure of HBT is taking place. Note that the SCCC and NCCC angles of the starting intermolecular hydrogen-bonded structure are already significantly twisted by about 30° when the molecule is photoexcited (Table 2). At the beginning of the dynamics, only the NCCC angle changes significantly, while the SCCC angle remains approximately constant in the first 80 fs. This means that the torsional process is non-rigid, which is also observed in the previous work in the gas phase.[18] Furthermore, NCCC increases in the first 50 fs, then rotates back by about 10° and starts to increase again after about 80 fs. This oscillation in the NCCC angle occurs between PT2 (~50 fs) and keto (~116 fs). Because of limitations of the TDDFT method to describe such twisted structures, the dynamics close to conical intersections and the possibility of internal conversion were not further investigated.

To determine whether excited-state proton transfer (PT) or excited-state hydrogen atom transfer (HT) occurs in the dynamics of the ESInterPT-2W process in HBT–$(H_2O)_3$, the relative energies and possible crossings between the $^1\pi\pi^*$ and $^1\pi\sigma^*$ states were computed along the trajectory illustrated in Fig. 4. The shape of the molecular orbitals involved in the electronic excitations is shown in Fig. 8. The π and π* orbitals are completely localized on HBT whereas the σ* orbital shows partial charge-transfer character to the water molecules. The $^1\pi\pi^*$ and $^1\pi\sigma^*$ states play a key role in determining the nature of the excited state reaction, since PT should occur in the $^1\pi\pi^*$ state, while the HT due to charge transfer to the water molecules should occur through the $^1\pi\sigma^*$ state. For further discussion on PT *vs.* HT in excited states see ref. 38, 53 and 54.

In Fig. 9, the ground singlet (S_0) and excited singlet ($^1\pi\pi^*$ and $^1\pi\sigma^*$) state energies calculated using TDDFT/B3LYP/SVP-SV along the proton transfer pathway up to about 150 fs are plotted. The results indicate that there is no crossing between excited singlet $^1\pi\pi^*$ and $^1\pi\sigma^*$ states. We also compare the TDDFT excitation energies as listed in Table 5 for 8 configurations along the proton transfer pathway given in Fig. 6 with RI-CC2 results using the TZVP+sp basis set. These results, which show good agreement between RI-CC2 and TDDFT levels, make clear that along this pathway the energy of the $^1\pi\sigma^*$ state lies well above that of the $^1\pi\pi^*$ state with no conical intersections or avoided crossings occurring between them. This implies that the dynamics along

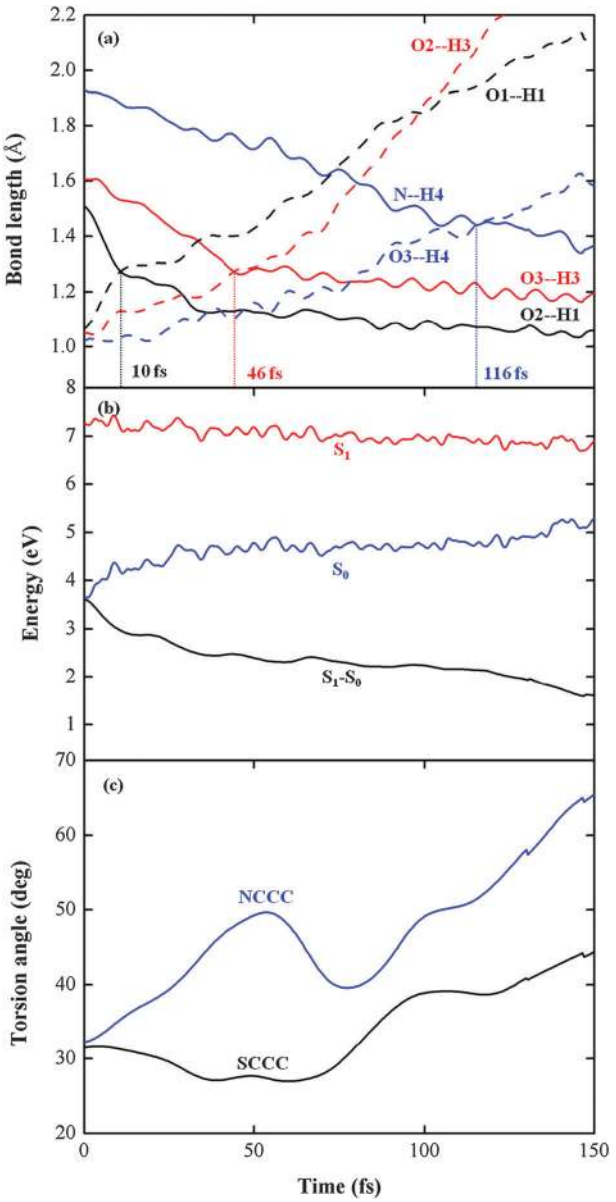

Fig. 7 (a) Time evolution of average bond breaking distances O1···H1, O2···H3 and O3···H4, and bond forming distances O2···H1, O3···H3 and N···H4 distances. (b) Average S_1 and S_0 energies and average energy differences between S_1 and S_0 states. (c) Average torsional angles SCCC and NCCC.

the S_1 state is a proton transfer process. Note that the results reported in Table 5 have been obtained for a single trajectory for methodological comparison only. They should not be taken as representative of energy barriers occurring on the energy surfaces.

As already mentioned, 10% of the trajectories reached a S_1/S_0 crossing prior to any proton transfer. This is also an indication that internal conversion may take place for this fraction of the population. Again due to limitations of the current approach, we could not further investigate this process. We can, however, report that these early intersections are caused either by O2–H or by O4–H dissociation, promoting n–π* or π–σ* crossings. These processes should be restricted to finite clusters, where dissociation

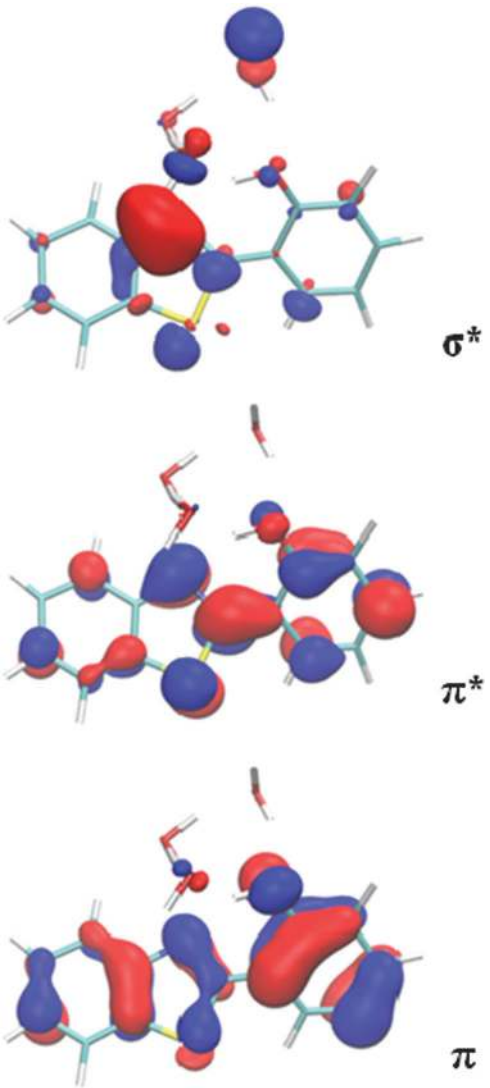

Fig. 8 Kohn–Sham orbitals computed at the DFT/B3LYP/SVP + sp-SV level characterizing the different electronic transitions involved in the PT and HT pathways. The enol geometry at 0 fs from Fig. 6 was used.

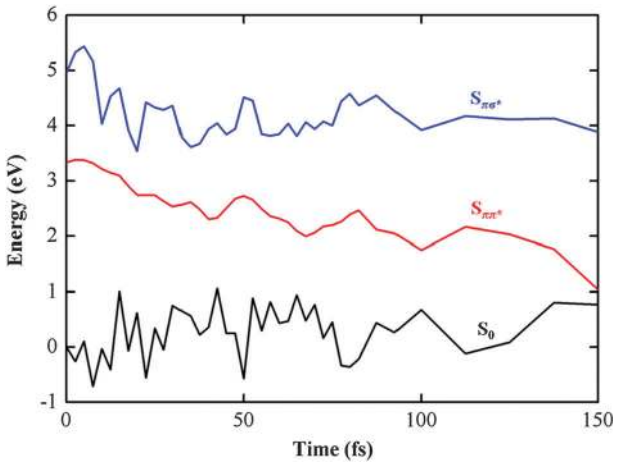

Fig. 9 Energy of the ground (S_0) and excited ($^1\pi\pi^*$, $^1\pi\sigma^*$) states evolving with time of a selected trajectory (the same trajectory as in Fig. 4) calculated at TD-B3LYP/SVP-SV/SVP-SV.

Table 5 Relative energies (eV) of the ground (S_0) and singlet-excited $\pi\pi^*$ and $\pi\sigma^*$ states for characteristic structures of a representative trajectory illustrated in Fig. 6, using the TD-DFT/B3LYP/SVP-SV and RI-CC2/TZVP + sp methods[a]

State	Method	Enol	IS1	PT1	IS2	PT2	IS3	Keto
S_0	TD-DFT	0.0	0.564	−0.084	1.120	1.049	0.616	0.581
	RI-CC2	0.0	0.875	0.232	1.450	1.202	0.897	0.805
$S_{\pi\pi^*}$	TD-DFT	3.328	3.315	2.906	2.627	2.361	1.992	2.200
	RI-CC2	3.537	3.338	3.125	2.870	2.432	2.015	2.183
$S_{\pi\sigma^*}$	TD-DFT	4.634	4.664	3.917	4.218	3.816	4.060	4.004
	RI-CC2	5.015	5.025	4.531	4.625	4.182	4.285	4.521

[a] RI-CC2/TZVP + sp calculations performed at B3LYP/SVP-SV geometries.

can effectively occur. In bulk water, early OH dissociation should not contribute significantly to internal conversion yield, since the dissociation would be replaced by inter-water proton transfer.

4 Conclusions

We have systemically investigated the structures of several HBT–water complexes to model the influence of hydrogen bonded interactions on the excited-state proton transfer. Two different solvent structures have been discussed in our investigations: intra- and intermolecular hydrogen-bonded structures. In the former structure, the intramolecular hydrogen bond in HBT remained intact, whereas, in the latter case, the proton of the OH group of HBT formed hydrogen bonds with the water molecule. From our thermodynamic calculations both structures are likely to co-exist.

Excited-state dynamics simulations were performed to study in detail the different excited-state proton transfer pathways associated with the enol → keto tautomerization using the HBT–$(H_2O)_3$ cluster as a representative model. The analysis of the dynamics simulations gives interesting insight into the different available proton transfer pathways and allows also their classification in terms of respective time constants. The consequences concerning internal conversion to the electronic ground state have also been discussed.

If the excited-state dynamics starts with the intramolecular hydrogen-bonded enol tautomer, a homogeneous ESIPT mechanism is observed to take place within only 18 fs, which is twice as fast as that in the gas phase computed at the same level. This speedup can be explained by the stronger intramolecular hydrogen bond in the HBT–$(H_2O)_3$ cluster as compared to isolated HBT.[18] Different from this case, the photodynamics of the intermolecular hydrogen-bonded enol tautomer is more complex, involving several distinct mechanisms. The main process, accounting for 76% of the computed trajectories, shows the tautomerization process proceeding *via* a triple proton transfer through the water network. This process takes significantly longer than in the intramolecular case, with an average time of approximately 120 fs. Due to the lack of the stabilizing hydrogen bond, intermolecular hydrogen-bonded structures have a significant degree of interring twisting of HBT already in the ground state. During the excited state dynamics, this twist tends to quickly increase, bringing the complex to a region of intersection between the S_1 and S_0 states. This situation indicates that internal conversion to the electronic ground state should take place at the sub-picosecond scale, explaining the experimentally observed low intensity of the keto emission.[76]

Our investigations also indicate that the intermolecular excited-state proton transfer in the first excited state proceeds along a pathway which is of $^1\pi\pi^*$ character with the electronic excitation located within the π system of HBT. No crossing between $^1\pi\pi^*$ and $^1\pi\sigma^*$ states is observed. Thus, these transfer processes are classified as proton transfer and not as hydrogen transfer.

Acknowledgements

This work is supported by the Austrian Science Fund within the framework of the Special Research Program F41 Vienna Computational Materials Laboratory (ViCoM). N.K. is grateful to the Austrian Exchange Service (OEAD) for a postdoc fellowship. The calculations were partially performed at the computer system of the Vienna Science Cluster (VSC). This work was also performed as part of research supported by the National Science Foundation Partnership in International Research and Education (PIRE) Grant No. OISE-0730114; support was also provided by the Robert A. Welch Foundation under Grant No. D-0005.

References

1 L. G. Arnaut and S. J. Formosinho, *J. Photochem. Photobiol., A*, 1993, **75**, 1.
2 A. L. Sobolewski and W. Domcke, *J. Phys. Chem. A*, 2007, **111**, 11725.
3 S. J. Formosinho and L. G. Arnaut, *J. Photochem. Photobiol., A*, 1993, **75**, 21.
4 P.-T. Chou, S. L. Studer and M. L. Martinez, *Appl. Spectrosc.*, 1991, **45**, 513.
5 T. Kim, H. J. Kang, G. Han, S. J. Chung and Y. Kim, *Chem. Commun.*, 2009, 5895.
6 A. R. Morales, K. J. Schafer-Hales, C. O. Yanez, M. V. Bondar, O. V. Przhonska, A. I. Marcus and K. D. Belfield, *ChemPhysChem*, 2009, **10**, 2073.
7 F. S. Rodembusch, F. P. Leusin, L. F. da Costa Medina, A. Brandelli and V. Stefani, *Photochem. Photobiol. Sci.*, 2005, **4**, 254.
8 S. M. Chang, Y. J. Tzeng, S. Y. Wu, K. Y. Li and K. L. Hsueh, *Thin Solid Films*, 2005, **477**, 38.
9 S. M. Chang, K. L. Hsueh, B. K. Huang, J. H. Wu, C. C. Liao and K. C. Lin, *Surf. Coat. Technol.*, 2006, **200**, 3278.
10 S. Lochbrunner, K. Stock and E. Riedle, in *Hydrogen-Transfer Reactions*, ed. J. T. Hynes, J. P. Klinman, H.-H. Limbach and R. L. Schowen, Wiley-VCH, Weinheim, Germany, 2006.
11 S. Lochbrunner, A. J. Wurzer and E. Riedle, *J. Chem. Phys.*, 2000, **112**, 10699.
12 S. Lochbrunner, A. J. Wurzer and E. Riedle, *J. Phys. Chem. A*, 2003, **107**, 10580.
13 S. Lochbrunner, K. Stock and E. Riedle, *J. Mol. Struct.*, 2004, **700**, 13.
14 R. De Vivie-Riedle, V. De Waele, L. Kurtz and E. Riedle, *J. Phys. Chem. A*, 2003, **107**, 10591.
15 D. Sun, J. Fang, G. Yu and F. Ma, *THEOCHEM*, 2007, **806**, 105.
16 M. A. Rios and M. C. Rios, *J. Phys. Chem. A*, 1998, **102**, 1560.
17 C. A. S. Potter, R. G. Brown, F. Vollmer and W. Rettig, *J. Chem. Soc., Faraday Trans.*, 1994, **90**, 59.
18 M. Barbatti, A. J. A. Aquino, H. Lischka, C. Schriever, S. Lochbrunner and E. Riedle, *Phys. Chem. Chem. Phys.*, 2009, **11**, 1406.
19 O. F. Mohammed, S. Luber, V. S. Batista and E. T. J. Nibbering, *J. Phys. Chem. A*, 2011, **115**, 7550.
20 H. Wang, H. Zhang, O. K. Abou-Zied, C. Yu, F. E. Romesberg and M. Glasbeek, *Chem. Phys. Lett.*, 2002, **367**, 599.
21 C.-C. Hsieh, Y.-M. Cheng, Y.-M. Hsu, K.-Y. Chen and P.-T. Chou, *J. Phys. Chem. A*, 2008, **112**, 8323.

22 C. Schriever, M. Barbatti, K. Stock, A. J. A. Aquino, D. Tunega, S. Lochbrunner, E. Riedle, R. De Vivie-Riedle and H. Lischka, *Chem. Phys.*, 2008, **347**, 446.
23 P.-T. Chou, Y.-C. Chen, W.-S. Yu, Y.-H. Chou, C.-Y. Wei and Y.-M. Cheng, *J. Phys. Chem. A*, 2001, **105**, 1731.
24 S. Takeuchi and T. Tahara, *J. Phys. Chem. A*, 2005, **109**, 10199.
25 C. Chudoba, S. Lutgen, T. Jentzsch, E. Riedle, M. Woerner and T. Elsaesser, *Chem. Phys. Lett.*, 1995, **240**, 35.
26 A. L. Sobolewski, W. Domcke and C. Hättig, *J. Phys. Chem. A*, 2006, **110**, 6301.
27 F. Plasser, M. Barbatti, A. J. A. Aquino and H. Lischka, *J. Phys. Chem. A*, 2009, **113**, 8490.
28 K. Stock, C. Schriever, S. Lochbrunner and E. Riedle, *Chem. Phys.*, 2008, **349**, 197.
29 J. M. Ortiz-Sanchez, R. Gelabert, M. Moreno and J. M. Lluch, *ChemPhysChem*, 2007, **8**, 1199.
30 A. Douhal, F. Lahmani and A. H. Zewail, *Chem. Phys.*, 1996, **207**, 477.
31 P. Purkayastha and N. Chattopadhyay, *Phys. Chem. Chem. Phys.*, 2000, **2**, 203.
32 R. S. Becker, C. Lenoble and A. Zein, *J. Phys. Chem.*, 1987, **91**, 3509.
33 C. Schriever, S. Lochbrunner, E. Riedle and D. J. Nesbitt, *Rev. Sci. Instrum.*, 2008, **79**, 13107.
34 Y.-M. Cheng, S.-C. Pu, C.-J. Hsu, C.-H. Lai and P.-T. Chou, *ChemPhysChem*, 2006, **7**, 1372.
35 Y. Nosenko, A. Kyrychenko, R. P. Thummel, J. Waluk, B. Brutschy and J. Herbich, *Phys. Chem. Chem. Phys.*, 2007, **9**, 3276.
36 Y. Nosenko, M. Kunitski, C. Riehn, R. P. Thummel, A. Kyrychenko, J. Herbich, J. Waluk and B. Brutschy, *J. Phys. Chem. A*, 2008, **112**, 1150.
37 K. Sakota, C. Okabe, N. Nishi and H. Sekiya, *J. Phys. Chem. A*, 2005, **109**, 5245.
38 A. L. Sobolewski and W. Domcke, *J. Phys. Chem. A*, 2001, **105**, 9275.
39 M. S. Gordon, *J. Phys. Chem.*, 1996, **100**, 3974.
40 G. M. Chaban and M. S. Gordon, *J. Phys. Chem. A*, 1999, **103**, 185.
41 R. Casadesus, M. Moreno and J. M. Lluch, *Chem. Phys.*, 2003, **290**, 319.
42 A. Hara, K. Sakota, M. Nakagaki and M. Sekiya, *Chem. Phys. Lett.*, 2005, **407**, 30.
43 K. Sakota, N. Inoue, Y. Komoto and H. Sekiya, *J. Phys. Chem. A*, 2007, **111**, 4596.
44 K. Sakota, Y. Kageura and H. Sekiya, *J. Chem. Phys.*, 2008, **129**, 054303.
45 K. Sakota, N. Komure, W. Ishikawa and H. Sekiya, *J. Chem. Phys.*, 2009, **130**, 224307.
46 R. Daengngern, N. Kungwan, P. Wolschann, A. J. A. Aquino, H. Lischka and M. Barbatti, *J. Phys. Chem. A*, 2011, **115**, 14129.
47 Y. Koizumi, C. Jouvet, T. Norihiro, S.-I. Ishiuchi, C. Dedonder-Lardeux and M. Fujii, *J. Chem. Phys.*, 2008, **129**, 104311.
48 W.-H. Fang, *J. Am.Chem. Soc.*, 1998, **120**, 7568.
49 Y. Matsumoto, T. Ebata and N. Mikami, *J. Phys. Chem. A*, 2002, **106**, 5591.
50 O.-H. Kwon, Y.-S. Lee, B. K. Yoo and D.-J. Jang, *Angew. Chem., Int. Ed.*, 2006, **45**, 415.
51 N. Al-Lawatia, J. Husband, T. Steinbrecher and O. K. Abou-Zied, *J. Phys. Chem. A*, 2011, **115**, 4195.
52 C. Tanner, C. Manca and S. Leutwyler, *Science*, 2003, **302**, 1736.
53 C. Tanner, C. Manca and S. Leutwyler, *J. Chem. Phys.*, 2005, **122**, 204326.
54 I. Georgieva, N. Trendafilova, A. J. A. Aquino and H. Lischka, *J. Phys. Chem. A*, 2007, **111**, 127.
55 Y.-H. Liu, M. S. Mehata and J.-Y. Liu, *J. Phys. Chem. A*, 2011, **115**, 19.
56 D. Kina, A. Nakayama, T. Noro, T. Taketsugu and M. S. Gordon, *J. Phys. Chem. A*, 2008, **112**, 9675.
57 M. Guglielmi, I. Tavernelli and U. Rothlisberger, *Phys. Chem. Chem. Phys.*, 2009, **11**, 4549.
58 A. D. Becke, *Chem. Phys.*, 1993, **98**, 5648.
59 P. J. Stephens, F. J. Devlin, C. F. Chabalowski and M. J. Frisch, *J. Phys. Chem.*, 1994, **98**, 11623.
60 A. Schaefer, H. Horn and R. Ahlrichs, *J. Chem. Phys.*, 1992, **97**, 2571.
61 A. J. A. Aquino, D. Tunega, G. Haberhauer, M. H. Gerzabek and H. Lischka, *J. Phys. Chem. A*, 2002, **106**, 1862.
62 C. Moller and M. S. Plesset, *Phys. Rev.*, 1934, **46**, 618.
63 F. Weigend and M. Haser, *Theor. Chem. Acc.*, 1997, **97**, 331.
64 F. Weigend, M. Haser, H. Patzelt and R. Ahlrichs, *Chem. Phys. Lett.*, 1998, **294**, 143.
65 O. Christiansen, H. Koch and P. Jorgensen, *Chem. Phys. Lett.*, 1995, **243**, 409.
66 A. Kohn and C. Hättig, *J. Chem. Phys.*, 2003, **119**, 5021.
67 C. Hättig, *J. Chem. Phys.*, 2003, **118**, 7751.
68 R. Ahlrichs, M. Baer, M. Haeser, H. Horn and C. Koelmel, *Chem. Phys. Lett.*, 1989, **162**, 165.
69 M. E. Casida, *Recent Advances in Computational Chemistry*, 1995, **1**, 155.
70 R. Bauernschmitt and R. Ahlrichs, *Chem. Phys. Lett.*, 1996, **256**, 454.
71 F. Furche and R. Ahlrichs, *J. Chem. Phys.*, 2002, **117**, 7433.
72 E. Runge and E. K. U. Gross, *Phys. Rev. Lett.*, 1984, **52**, 997.
73 A. J. A. Aquino, M. Lischka and C. Hättig, *J. Phys. Chem. A*, 2005, **109**, 3201.
74 M. Barbatti, G. Granucci, M. Persico, M. Ruckenbauer, M. Vazdar, M. Eckert-Maksic and H. Lischka, *J. Photochem. Photobiol., A*, 2007, **190**, 228.
75 M. Barbatti, G. Granucci, M. Ruckenbauer, F. Plasser, J. Pittner, M. Persico and H. Lischka, *NEWTON-X: a packagefor Newtonian dynamics close to the crossing seam*, 2011, www.newtonx.org.
76 R. Wang, D. Liu, K. Xu and J. Li, *J. Photochem. Photobiol., A*, 2009, **205**, 61.